

Crystal Structures of Two-Dimensional Binary Mixtures of Dipolar Colloids in Tilted External Magnetic Fields

Alexandros Chremos^{*,†} and Christos N. Likos[‡]

School of Chemistry, University of Edinburgh, West Mains Road, Edinburgh EH3 9JJ, United Kingdom, and Institute for Theoretical Physics II: Soft Matter, Heinrich-Heine-Universität Düsseldorf, Universitätsstrasse 1, D-40225 Düsseldorf, Germany

Received: April 25, 2009; Revised Manuscript Received: June 10, 2009

We employ genetic algorithms, which allow for an efficient search for the global minimum of energy landscapes, to investigate the ordered equilibrium structures formed by a binary mixture of anisotropic dipolar particles confined on a plane, under the influence of an external magnetic field. The anisotropy is introduced by titling the external field with respect to the interface, and it is tuned by the degree of the tilt angle. For small tilt angles, the structures obtained for perpendicular fields are slightly perturbed but beyond system-dependent values of the tilt, novel structures emerge, characterized by the formation of complex arrangements of chains that lie parallel to the in-plane projection of the field.

I. Introduction

The crystallization of colloids confined at liquid–air and liquid–liquid interfaces has recently attracted a great deal of attention^{1–11} due to the large number of potential applications ranging from food and agrochemicals to petrochemicals and pharmaceuticals. Unlike particles in the bulk, the effective interactions between colloidal particles at fluid interfaces are influenced not only by the properties of the particles and the solvent but also by the surface and line tensions of the interface.¹⁰

Among the various experimental setups of binary mixtures of dipolar colloids, two such realizations are related with this work and we briefly describe them here. The first realization deals with colloidal dipoles, which are roughly spherical particles with diameters in the range 10 nm to 1 μm . To prevent irreversible aggregation, the particles are usually coated with a thin layer of nonmagnetic material. Thus the net colloid–colloid interaction is mainly dipolar, with the coatings providing a relatively weak short-range dispersion interactions. The colloidal dipoles are suspended in a pendant drop in gravity¹² (system I); see Figure 1a. In the second, colloids of polystyrene float on an oil–water interface¹¹ (system II); see Figure 1b. The colloids are trapped at the oil–water interface because this way they minimize the surface between the two phases. Nevertheless, the polystyrene colloids do not have a molecularly smooth surface and water molecules are trapped at the colloid–oil interface. This has as a consequence the formation of water droplets or a thin film surrounding the polystyrene colloid with dipoles. The net dipole moment of the dipoles surrounding the colloid is nonzero, because the dipole interaction is screened in the aqueous phase.

In the first case (system I, superparamagnetic colloids), one can apply an external magnetic field to induce a tunable colloid–colloid interaction, whose direction and strength can easily be controlled via the external field; the dipole moments almost perfectly align along the field direction, and the

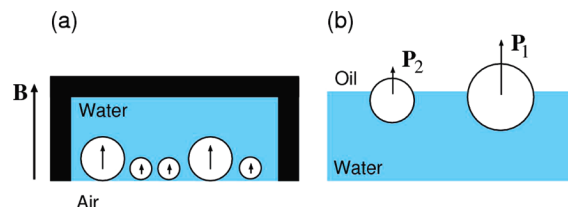


Figure 1. Schematic illustration of system I and system II. (a) System I: two superparamagnetic colloids of different sizes trapped at the air–water interface of a pendant water droplet. An external magnetic field \mathbf{B} is applied, shown in this case in a direction perpendicular to the confining plane, and it induces magnetic dipoles on the colloids, indicated by the arrows inside the white circles. (b) System II: Two colloids of different sizes trapped at the oil–water interface. The dipole moments \mathbf{P}_1 and \mathbf{P}_2 are given by the vector sum of the dipole moments on the particle–oil interface.

magnitude of the dipole moment is proportional to the field strength. In the conventional setup, the field is perpendicular to the interface, inducing a repulsive interaction between the colloids, additional to the short-ranged steric repulsion arising from the physical cores of the colloids. For large fields, the typical strength of the repulsive dipole–dipole interaction is much larger than the thermal energy, leading to crystallization of the colloids. In the second case (system II), dipoles form spontaneously due to the fact that the colloids are partly immersed in an organic solvent and partly in a polar one (water). Both realizations have been extensively studied in experiments,^{1,3–7,12–19} as well as in theory and simulations.^{2,6,8,9,11,20} As shown in refs 8 and 9, at sufficiently low density the dipole–dipole interactions of system I and II become equivalent. In the work at hand, we focus on superparamagnetic colloids, for which not only the magnitude but also the *direction* of the induced dipoles can be influenced, in particular by titling the field with respect to the direction perpendicular to the interface, inducing thereby anisotropic interactions.

Another experimental realization of two-dimensional particle arrangements occurs through the deposition or adsorption of colloidal particles on hard, air–solid interfaces.^{22–26} Depending on the particle size, the surface might be considered as smooth

* Corresponding author. Present address: Department of Chemical Engineering, Princeton University, Princeton NJ 08540.

† University of Edinburgh.

‡ Heinrich-Heine-Universität Düsseldorf.

(if the particles are much larger than atomic dimensions) or it must be resolved on the atomic scale. The particle–surface interactions would, in the last case, play an additional role in determining the equilibrium structures, and the same holds true for the effects of surface curvature.²⁷ In this work, we focus on magnetic colloids at fluid–fluid interfaces instead, for which it has been shown⁶ that the dipolar potential accurately describes the interparticle interactions.

The dipolar pair interactions of colloids of a binary mixture of big (A) and small (B) particles, having diameters σ_A and σ_B , respectively, have the form of a power law. Scaling interparticle separations r with the large diameter and introducing thereby the dimensionless variable $x \equiv r/\sigma_A$, the dipolar interactions for perpendicular fields, $\Phi_{ij}^\perp(r)$, take the form⁹

$$\Phi_{ij}^\perp(r) = E_M \frac{m_i m_j}{x^3} \quad (1)$$

where $i, j = A, B$, $m_i = \chi_i/\chi_A \leq 1$ is the ratio of the magnetic susceptibility of particle i to that of the large particle, and the magnetic energy scale E_M is given by

$$E_M = \frac{\mu_0 \chi_A^2 |\mathbf{B}|^2}{4\pi \sigma_A^3} \quad (2)$$

with the magnetic permeability of vacuum μ_0 and the external magnetic field \mathbf{B} .

It is desirable to relate the susceptibility ratio to the size asymmetry $z_i = \sigma_i/\sigma_A \leq 1$ between the two species. For these purposes, in ref 9, the assumption was made that the susceptibility of a colloid scales with its size as $\chi_i \propto \sigma_i^{(n+2)/2}$. The exponent $n = 2$ corresponds to surface doping with ferromagnetic material, so that $\chi_i \propto \sigma_i^2$, whereas volume doping, $\chi_i \propto \sigma_i^3$ results for the choice $n = 4$. Since neither is strictly true for the colloids at hand, here we adopt the value $n = 3$ and note that, as shown in ref 9, for power-law interactions different choices for n are related to one another by simple rescaling. Under this assumption, the isotropic, dipolar interactions of eq 1 take the form

$$\Phi_{ij}^\perp(r) = E_M \frac{(z_i z_j)^{5/2}}{x^3} \quad (3)$$

Knowing the effective interactions between the particles one can use computer simulations to obtain the minimum energy configuration (MEC), and thus the favored crystal structure at $T = 0$. However, it is well-known that binary mixtures tend to exhibit a broad spectrum of rather complex alloy phases²¹ corresponding to a very rough energy landscape; few optimization algorithms are able to solve such high-dimensional and complex problems. To overcome this difficulty, genetic algorithms (GAs) have been applied to the case of binary mixtures with their interactions described by eq 1. The results revealed a rich spectrum of exotic ordered ground state structures.^{8,9}

The main focus of the current work is to explore, with the use of GA, the crystal structures emerging from a binary mixture of colloids when the external field is tilted with respect to the normal of the interface. The tilt angle introduces an anisotropic interaction creating new exotic crystal structures. As the field is tilted beyond a critical angle, the patterns switch over being dominated by chains aligned parallel to the field.

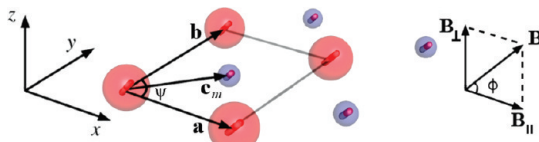


Figure 2. Schematic drawing of the setup of two-dimensional superparamagnetic colloidal particles under an external magnetic field \mathbf{B} , which is tilted with respect to the confining plane of the particles. For a description of the geometry, see the text.

The paper is organized as follows. In section II A we define our model and in section III the method applied to investigate the ordered structures, which is based on genetic algorithms. The results are presented and discussed in section IV. Finally, in section V we summarize the conclusions.

II. The Model and the Interaction Potentials

A. Lattice Parameters. We consider a binary mixture of particles, namely type A and B, with their diameter ratio, $z \equiv z_B = \sigma_B/\sigma_A = 0.5$, unless stated otherwise. To determine the global energy minimum of such a system, we assume that the particles arrange themselves in a set of Bravais lattices. Specifically, we consider a two-dimensional Bravais lattice with an s -particle unit cell, where s is the sum of n_A particles of type A and n_B particles of type B.

The candidate structures are generated by the periodic repetition of the unit cell, which is a parallelogram formed by the vectors \mathbf{a} and \mathbf{b} that sustain an angle ψ between them; see Figure 2. The colloids are confined on the (x, y) -plane, whereas the external field is taken to lie on the (x, z) plane, without loss of generality, as shown on the right part of the picture. Due to the superparamagnetic nature of the colloids, each one develops a magnetic moment that lies parallel to \mathbf{B} and is denoted by the tiny “magnets” in the interior of the particles in the middle of the figure. We have plotted for demonstration two types of superparamagnetic particles, distinguished by their magnetic susceptibilities, as red and blue transparent spheres. Particles of type A (red) order on a crystalline lattice with lattice vectors \mathbf{a} and \mathbf{b} , while other particles occupy identical sublattices, shifted with respect to the first one by the vectors \mathbf{c}_m . Anticipating the results of the search algorithm, one crystallographic direction, lying along the \mathbf{a} -Bravais lattice vector, has been chosen to be along the projection $\mathbf{B}_{||}$ of the tilted field on the confining plane, which is also the x -axis of the Cartesian coordinate system.

For convenience, but without loss of generality, we set the particles occupying vertices of the parallelogram to be of type A, and their positions are described by the linear combinations $\mathbf{R}_{kl} = k\mathbf{a} + l\mathbf{b}$, where k and l are integers. We introduce a coordinate system (x, y) and because the x axis is parallel to the unit-cell vector \mathbf{a} , the primitive vectors of the Bravais lattice take the form

$$\begin{aligned} \mathbf{a} &= \alpha(x, 0) \\ \mathbf{b} &= \alpha(\cos \psi, \sin \psi) \end{aligned} \quad (4)$$

where x is a variable determining the length of \mathbf{a} vector, $|\mathbf{a}| = x|\mathbf{b}|$, and α is a scaling variable defined by the number density as $\rho = s/|\mathbf{a} \times \mathbf{b}| = s/(x\alpha^2 \sin \psi)$. Now, since ρ will be fixed, it allows the elimination of one parameter of our model, $\alpha = [N/(x\rho \sin \psi)]^{1/2}$. We call the lattice just described as the *primary lattice*. The additional particles of the unit cell, which can be of type A or B, are placed inside the parallelogram, and their positions are specified by the set of vectors $\mathbf{c}_m = c_m^a \mathbf{a} + c_m^b \mathbf{b}$,

where $c_m^{a,b}$ are coefficients and m is the index of the additional particles, $m = 2, \dots, s$; the value $m = 1$ is reserved for the coordinates of the particle belonging to the first-lattice, $\mathbf{c}_1 = (0, 0)$. When such a cell is repeated periodically over space, it produces s identical sublattices, each of them being shifted with respect to the first-lattice by the vectors \mathbf{c}_m .

Let now $\Phi_{ij}(\mathbf{r})$ be the interparticle pair potential between species i and j . According to the discussion above, n_A of the s identical sublattices will be occupied by particles of type A, whereas the remaining n_B ones by particles of the type B. The relative positions of the particles in the primitive lattice, as well as in its $s - 1$ repetitions that are shifted with respect to it by the basis vectors \mathbf{c}_m , $m = 2, 3, \dots, s$, consist of all linear combinations $\mathbf{R}_{kl} = k\mathbf{a} + l\mathbf{b}$ with integer coefficients k and l . It is straightforward to show that for a system containing a total of N particles, the total energy per particle of the candidate lattice, $u \equiv U/N$, is given by the expression⁹

$$\begin{aligned} u = & \frac{n_A}{2s} \sum_{k \neq 0} \sum_{l \neq 0} \Phi_{AA}(k\mathbf{a} + l\mathbf{b}) + \\ & \frac{n_B}{2s} \sum_{k \neq 0} \sum_{l \neq 0} \Phi_{BB}(k\mathbf{a} + l\mathbf{b}) + \\ & \frac{1}{s} \sum_k \sum_l \sum_{m=1}^{s-1} \sum_{n=m+1}^s \Phi_{\epsilon(m)\epsilon(n)}(k\mathbf{a} + l\mathbf{b} + \mathbf{c}_m - \mathbf{c}_n) \end{aligned} \quad (5)$$

where the type of interaction in the last term is determined by the occupancy of the sublattice by the particle species involved: $\epsilon(m) = A$ for $1 \leq m \leq n_A$ and $\epsilon(m) = B$ for $n_A < m \leq s$.

Hence, the parameters that characterize the structure of the lattice are s , ρ , x , and ψ , as well as the components of the basis vectors along the directions of \mathbf{a} and \mathbf{b} , c_m^a and c_m^b , $m = 2, 3, \dots, s$. These parameters are subject to the following constraints:

$$0 < x \leq 1, \quad 0 < \psi \leq \pi/2, \quad 0 \leq c_m^{a,b} \leq 1 \quad (6)$$

Note that the representation in eq 4, even with the above constraints, is *not* unique, since different sets of parameters can create equivalent structures; these ambiguities are settled by employing a suitable selection algorithm described in section IIIC.

In the following, we characterize the composition of the binary mixture by the mole fraction of small particles, $C = n_B/s$. The parameter ranges we explore in this work are $\rho\sigma_A^2 = 0.4, 0.6$ and 0.8 and $C = 1/2, 2/3, 3/4, 4/5, 5/6, 1/3, 1/4$, and $1/5$. Larger unit cells of the same composition, e.g., $C = 2/4 = 1/2$, will be part of a future study. In what follows, we also set $\sigma_A = 1$ and simply quote the area density as ρ .

B. Interactions. As mentioned in the introduction, we study colloids with dipole–dipole interactions, and with an external magnetic field, \mathbf{B} , strong enough to create crystallization. The field is, in general, not perpendicular to the confining plane; i.e., the angle subtended between \mathbf{B} and the (x, y) -plane is $\phi \neq 90^\circ$, as shown in Figure 2. Before we analyze in detail the interactions between the particles, we define the two components of \mathbf{B} , one parallel to the plane of the interface, $\mathbf{B}_{||}$, and the other normal to the interface, \mathbf{B}_{\perp} ; see again Figure 2. There is no a priori reason why the in-plane component of the field should align itself parallel to a particular crystallographic direction of the ensuing lattice. However, since the magnetic repulsions

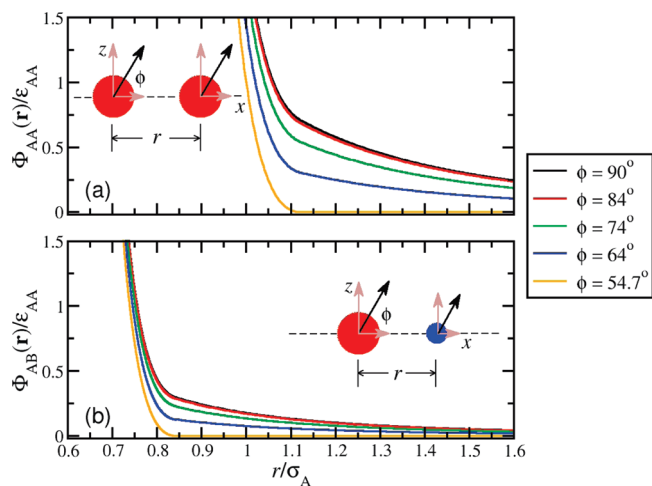


Figure 3. Dependence of the total interaction potential $\Phi_{AA}(\mathbf{r})$ between two big colloids [(a), upper panel] and of the interaction potential $\Phi_{AB}(\mathbf{r})$ between a big and a small colloid [(b), lower panel] on the interparticle separation r for fixed angle $\theta = 0$ and different external field angles ϕ , as indicated in the legend. The size ratio is here $z = 0.5$. The insets show sketches of two colloidal particles [(a) two big ones; (b) one big and one small], separated by a distance r . The colloids are confined on an interface, denoted by the dashed line, and an external magnetic field \mathbf{B} is imposed, oriented parallel to the black arrows. It induces dipole moments denoted by the black arrows, which can be decomposed on the perpendicular, z -direction and the in-plane, x -direction, indicated by the brown arrows. The connecting vector \mathbf{r} between the colloidal centers lies parallel to the in-plane projection of the magnetic field in this case, thus the dipoles have a “head-to-tail” configuration, and $\theta = 0$. The geometry is a side view of that sketched in Figure 2.

between the particles are weakest along the direction of $\mathbf{B}_{||}$ and can even be turned to attractions for sufficiently strongly tilted fields (see below), it turns out that $\mathbf{B}_{||}$ indeed aligns with one of the two primitive vectors. This is in full agreement with previous findings on the crystal structures of *one-component* paramagnetic systems in tilted fields.²⁸ Accordingly, in what follows we set the $\mathbf{B}_{||}$ parallel with the x -axis and the vector \mathbf{a} , so that the external field is expressed as $\mathbf{B} = |\mathbf{B}|(\cos \phi, 0, \sin \phi)$.

Following the considerations presented in ref 28, the dipole–dipole pair potential at the interface in the presence of a tilted magnetic field results as a generalization of the one given in eq 3 and reads

$$V_{\text{dipolar}}^{(ij)}(\mathbf{r}) = E_M \frac{(z_i z_j)^{5/2}}{x^3} (1 - 3 \cos^2 \phi \cos^2 \theta) \quad (7)$$

recovering the isotropic case, eq 3, for perpendicular fields, $\phi = 90^\circ$. Moreover, $\cos \theta = \mathbf{r} \cdot \mathbf{B}_{||}/(rB_{||})$, is the cosine of the angle θ formed between the connecting vector between two dipoles at separation \mathbf{r} and the in-plane component of the field; see Figure 2.

The degree of anisotropy is controlled via the tilt angle ϕ , as seen in Figure 3, which allows the particles to adopt less repulsive head-to-tail configurations, $\theta = 0$. In this work, we will restrict the tilt angle above the threshold value $\arccos(1/\sqrt{3}) \approx 54.7^\circ$; below that value, the dipole interactions in the head-to-tail configuration become attractive. The values investigated are $\phi = 54.7^\circ, 59^\circ, 64^\circ, 74^\circ$, and 84° . Additionally, we generate structures at 90° for comparison.

At a high degree of anisotropy, the particles will collapse to each other due to the absence of repulsive interactions along the x direction. On these grounds, and also with the purpose of

guaranteeing the stability of the system against implosion for the case $\phi < 54.7^\circ$ (not studied here), we also introduce short-range, isotropic, steric repulsions between the colloids. To model these, we employ the purely repulsive Weeks–Chandler–Andersen (WCA) potential,²⁹ which is a Lennard-Jones potential cut and shifted at the position of the minimum, $r_{\min} = 2^{1/6}\sigma_{ij}$. In particular, we add the steric potentials:

$$V_{\text{steric}}^{(ij)}(r) = \begin{cases} 4\epsilon_{ij} \left[\left(\frac{\sigma_{ij}}{r} \right)^{12} - \left(\frac{\sigma_{ij}}{r} \right)^6 \right] + \epsilon_{ij} & r \leq r_{\min} \\ 0 & r > r_{\min} \end{cases} \quad (8)$$

The steric interactions introduce three additional energy scales, ϵ_{AA} , ϵ_{AB} , and ϵ_{BB} , among all species, as well as three new length scales, σ_{AA} , σ_{AB} , and σ_{BB} . These are fixed as follows: to avoid large discrepancies between magnetic and steric energy scales, we equate the magnetic and steric energy scales of the large particles, and we assume that the latter scale proportionally to the particle's size, i.e.:

$$\begin{aligned} \epsilon_{AA} &= E_M \\ \epsilon_{BB} &= zE_M \end{aligned} \quad (9)$$

Further, we make the natural choice to set the steric, like-species interaction diameters σ_{AA} and σ_{BB} of the colloids equal to their physical diameters, i.e.:

$$\begin{aligned} \sigma_{AA} &= \sigma_A \equiv 1 \\ \sigma_{BB} &= \sigma_B \equiv z \end{aligned} \quad (10)$$

The remaining parameters of the steric interactions are fixed by employing the standard Lorentz–Berthelot mixing rules,³⁰ namely:

$$\begin{aligned} \epsilon_{AB} &= \sqrt{\epsilon_{AA}\epsilon_{BB}} = \sqrt{z}E_M \\ \sigma_{AB} &= \frac{\sigma_{AA} + \sigma_{BB}}{2} \end{aligned} \quad (11)$$

Combining eq 7 and eq 8 together, the total pair potential takes the form

$$\Phi_{ij}(\mathbf{r}) = V_{\text{dipolar}}^{(ij)}(\mathbf{r}) + V_{\text{steric}}^{(ij)}(r) \quad (12)$$

According to the above considerations, the relative energy and length scales of the three interactions are fully determined by the size ratio z . In Figure 3 we show a comparison of the total interaction potentials $\Phi_{AA}(\mathbf{r})$ (panel a) and $\Phi_{AB}(\mathbf{r})$ (panel b), for size ratio $z = 0.5$, fixing the head-to-tail configuration, $\theta = 0$, and focusing on their dependence on the field angle ϕ . The softening of the interaction as ϕ decreases from 90° can be seen, resulting even into an interaction that identically vanishes for large enough separation at the threshold value $\phi = 54.7^\circ$. Further, it can be seen that $\Phi_{AA}(\mathbf{r})$ has a stronger short-range repulsion than its unlike-species counterpart, $\Phi_{AB}(\mathbf{r})$. In Figure 4, on the other hand, we fix the interparticle separation between two particles of species A at a value slightly larger than the steric interaction cutoff, $r = 1.2\sigma_A \gtrsim 2^{1/6}\sigma_A$, and consider the dependence of $\Phi_{AA}(\mathbf{r})$ on the angle θ for different values of ϕ . At the threshold value $\phi = 54.7^\circ$ the anisotropy is most strongly

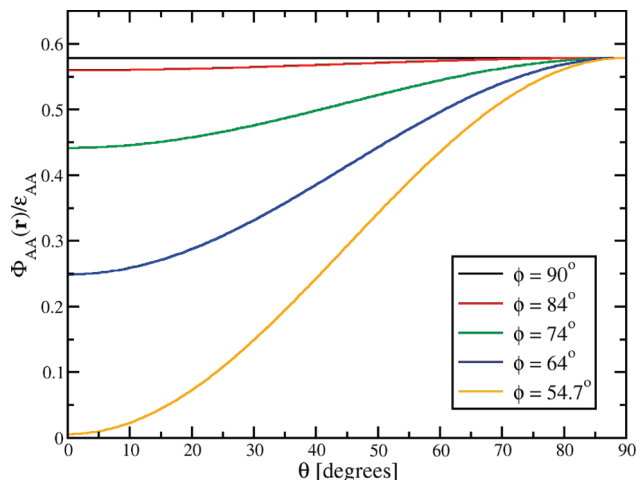


Figure 4. Total interaction potential $\Phi_{AA}(\mathbf{r})$ between two A type particles at fixed interparticle separation, $r = 1.2\sigma_A$, as a function of the angle θ between the connecting vector \mathbf{r} and the in-plane component of the magnetic field (x -axis), for different values of ϕ , as indicated in the legend.

present, decreasing as ϕ grows and disappearing altogether for the perpendicular field orientation, which obtains at $\phi = 90^\circ$. The energetically most favorable orientation of the dipoles results for $\theta = 0$, i.e., the head-to-tail configuration mentioned above.

III. Genetic Algorithms

A. Optimization Problems. Many interesting optimization problems require a reasonably fast and effective search and selection algorithm. Given a hard optimization problem, we need to search through a space of potential solutions either by finding, if possible, an efficient problem-specific algorithm which is approximately optimal, or by using probabilistic algorithms, which despite being powerful, do not guarantee to give the optimum solution. For small spaces, classical exhaustive methods usually suffice; for larger spaces special artificial intelligence techniques must be employed. GAs are stochastic search algorithms invented in the 1970s by Holland to solve high-dimensional and complex problems in engineering science.³¹ These methods are inspired by the Darwinian struggle for survival and employ evolutionary processes as key elements to obtain the optimal solution to a particular problem. However, strictly speaking, GAs like biological evolution do *not* optimize.^{31,32} Evolution uses whatever material that is at its disposal to produce above average individuals; it has no ultimate goal of “perfection”. Similarly, GAs do not *guarantee* convergence to the global minimum but they greatly accelerate the search for it and, due to their inherent ability to perform large jumps in search space, they can easily escape potential barriers in a rugged energy landscape. Accordingly, GAs form the basis of extremely robust optimization methods, which are able to take the whole search space into account, and at the same time concentrate their computing efforts on promising regions. For an overview, we refer the reader to ref 33.

B. Genetic Algorithms in General. We briefly summarize the basic ideas of a GA and in the subsequent section will show how it will be applied to our specific problem. A GA represents a candidate solution as an *individual*, whose *genes*, fixed in number, represent the variables of the given problem. The genes in an individual can take values from a suitably chosen alphabet, such as binary, with digits 0 and 1 as its letters. Usage of the binary alphabet is by no means compulsory, although it has

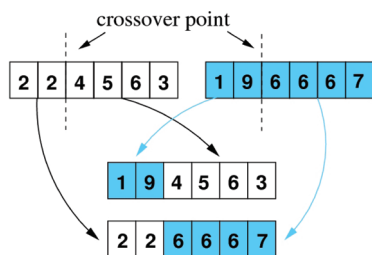


Figure 5. Schematic representation of the one-point crossover that generates two new individuals from two parents.

been extensively employed in previous works;^{8,9,34–38} here we will revert to the usual, decimal alphabet. All the genes together form the *chromosome* as a string of digits. Individuals are evaluated via a problem-specific fitness function, in the sense that a better or fitter individual has a higher fitness value. A large, but fixed, number of individuals form a generation.

The initialization of the GAs first generation is realized at random. A new generation is formed by selecting individuals to be parents from the former generation according to their fitness values, and then generating new individuals to form the subsequent generation. Several procedures for this mating and recombination processes have been proposed in the literature.³⁹ In addition, mutations are performed with a certain probability during the mating process, a procedure necessary to avoid persistent inbreeding and to allow at the same time for the reintroduction of new or lost genetic material. At each iteration selection-recombination-mutation-evaluation cycle, a fraction of the former generation is replaced to form the new generation. Usually, we retain individuals with the highest fitness value, but other replacement procedures exist. The final solution is represented by the fittest individual in the population after many generations.

C. Genetic Algorithms for Our Problem. These general ideas behind GAs are now applied to our problem of obtaining the optimal crystal structure of a binary mixture of colloidal particles, by using the model described in section II A. The formalism has been used in similar problems elsewhere in the literature.³⁴

We translate our model represented by the set of parameters $\{x, \Psi, c_1^a, c_2^a, \dots, c_s^a, c_s^b\}$, where $\Psi = \psi/(\pi/2)$, into an individual $\mathcal{I} = (\mathcal{I}_1, \mathcal{I}_2, \dots, \mathcal{I}_{2s-1}, \mathcal{I}_{2s})$, where $\mathcal{I}_1, \dots, \mathcal{I}_{2s}$ represent the parameters of our model as strings of genes of fixed length, $n_{\text{gene}} = 6$; see ref 41. The introduction of the scaled angle $\Psi = \psi/(\pi/2)$ is necessary, since in this way $\Psi \in [0, 1]$ as all other variational parameters of the problem. Indeed, the mating-recombination process to be described below “mixes” genes arbitrarily, so that it is crucial that the encoding of all parameters lie in the same interval. The genes are expressed by a decimal alphabet, i.e., an alphabet composed by the one-digit integers 0, 1, 2, ..., 9. The aim of the encoding is to produce a chromosome form, which the GA will use later. Taking now for the purposes of demonstration $s = 1$, the generated individual would result from a point in (y_1, y_2) space; the encoding process for two arbitrarily chosen values of y_1 and y_2 would produce

$$(y_1, y_2) = (0.122334, 0.988776) \rightarrow \\ \mathcal{I}_{y_1, y_2} = 122334988776 \quad (13)$$

For the present investigation, we used the number of individuals per generation $N_{\mathcal{G}} = 500$, and the number of generations $N_{\mathcal{G}} = 300$. Even though for most cases explored a smaller genetic

population would be sufficient to give a solution, a large population maintains diversity between individuals, covering thus the whole search space.

As mentioned in section II A, we need to implement an algorithm to ensure a unique representation of the Bravais lattice. This is achieved by requiring the perimeter of the unit cell, Π , to be minimal, and it is given by the equation

$$\Pi = 2(|\mathbf{a}| + |\mathbf{b}|) \quad (14)$$

To minimize the perimeter, eq 14, the following iterative algorithm was applied: the vectors \mathbf{a} and \mathbf{b} are replaced by new vectors, from the four options the combination with the lowest value out of Π ,

$$\{\mathbf{a} \pm \mathbf{b}, \mathbf{b}\} \quad \text{and} \quad \{\mathbf{a}, \mathbf{a} \pm \mathbf{b}\} \quad (15)$$

If none of the possible combinations minimize Π , then the algorithm stops and the initial \mathbf{a} and \mathbf{b} are used. The vectors \mathbf{c}_m are not required to be checked by the algorithm, since they are linear combinations of \mathbf{a} and \mathbf{b} .

A positive fitness value is assigned to each individual \mathcal{I} via the fitness function $f(\mathcal{I})$: a higher fitness value characterizes a better solution. The optimum solution is a crystal structure with the lowest free energy, $F = U - TS$, where S is entropy, but for our purposes we look for crystals formed by the system at zero temperature ($T = 0$). Therefore, the optimum crystal structure will have lowest potential energy, U , which can be calculated by eqs 5 and 12. Additionally, for practical reasons we look at the ratio $U(\mathcal{I})/U(\mathcal{I}^{\text{hex}})$, where $U(\mathcal{I}^{\text{hex}})$ is the potential energy of a hexagonal structure (hex) generated by one big particle per unit cell at the same density. The reason behind this is to ensure that the values used will be of order unity. Hence, $f(\mathcal{I})$, in our problem, reads

$$f(\mathcal{I}) = \exp \left\{ 1 - \frac{U(\mathcal{I})}{U(\mathcal{I}^{\text{hex}})} \right\} \quad (16)$$

Once the first generation, \mathcal{G}_0 , is realized and its individuals are evaluated by the fitting function, we sort them out by a ranking scheme. For example, the fittest individual will have rank value $R[f(\mathcal{I}_j)] = 1$, while the least fit will have $R[f(\mathcal{I}_j)] = N_{\mathcal{G}}$. This ranking scheme is important for avoiding breeding shortcomings and to ensure the existence of selection pressure throughout the simulation.³⁹

Afterward, the interactive process of creating a new generation starts. In the first step, two individuals are selected as parents according to the rank of their fitness values with the roulette wheel algorithm.³⁹ First, we generate a random number $w \in [0, S]$, where S is the sum of the differential fitnesses, S_j , over all the individuals in the population:

$$S = \sum_{j=1}^{N_{\mathcal{G}}} S_j = \sum_{j=1}^{N_{\mathcal{G}}} \frac{N_{\mathcal{G}} - R[f(\mathcal{I}_j)] + 1}{N_{\mathcal{G}}} \quad (17)$$

Now we use w to locate the element T_j in the following inequality,

$$T_{j-1} \leq w < T_j \quad (18)$$

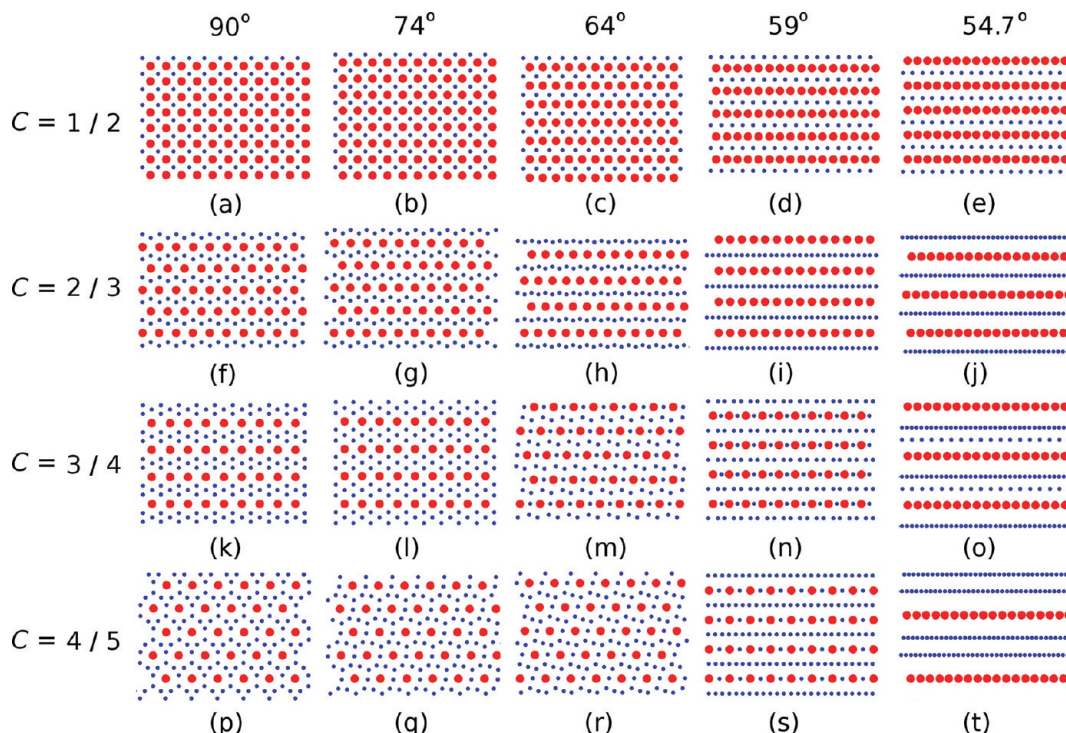


Figure 6. Minimum energy configurations for $C \geq 1/2$, density $\rho = 0.6$ and size ratio $z = 0.5$ at various values of the angle ϕ , as indicated in the plot. Red circles denote large particles and blue circles small ones.

where T_j is the running sum,

$$T_j = \sum_{l=1}^j S_l, \quad j = 1, \dots, N_{\mathcal{S}} \quad (19)$$

This procedure is equivalent to constructing a roulette wheel, where each individual is occupying a sector of angular size $2\pi S_l/S$ and the random number represents the spinning wheel. In other words, the probability of the wheel stopping at a sector is proportional to the sector's angular width. Once the parents are chosen, two new individuals populate the new generation via a one-point crossover, as visualized in Figure 5. The crossover point, which is randomly chosen, is where each of the parent's gene sequence is cut and combined to create the new individuals. This action is unbiased in respect to the geometry of the problem and cannot be associated with any physical movement of the particles. Further, we perform mutations with a probability p_m , which has a typical value of 0.1, on the new individuals. It means that we randomly choose one of the genes and replace it with a new one.

Even though the process of recombination and mutation will create two new individuals, it is not guaranteed that they will join the new generation. A number of criteria must be fulfilled. First, they must be at least as fit as the least-fit members of the existing population; the latter will be eliminated and replaced by the new members. Second, the new individuals must not be identical with any other member of the population; this *no-duplicate* criterion is an important safeguard against inbreeding.

It is obvious that with this representation the GAs are able to search all possible unit-cell shapes, while at the same time operating at the thermodynamic limit. This is a significant advantage over standard Monte Carlo annealing techniques. There, additional moves that adjust the shape of the simulation box for every envisioned lattice structure are necessary to avoid artifacts related to incommensurability between crystal structures

and simulation box that can severely influence the calculation of the solid free energy.

To test the efficiency of the reproduction strategy described above, it was compared to an alternative reproduction strategy in which we select parents randomly with no regard to fitness, and then randomly replace members of the population with the new individuals. An exception to this replacement is granted to the fittest individual, as a form of elitism. Strategies similar to this have been found advantageous for problems tending to suffer from premature convergence.⁴⁰ After the GA has provided a solution, a final optimization with gradient descent was applied. The last step was needed to increase the accuracy of the results.

IV. Results and Discussion

Here, we present the ordered equilibrium configurations obtained by the GA, as the angle of the magnetic field is tilted. The variables are the composition C of the mixture and the angle ϕ between the external magnetic field and the confining plane, whereas density ρ and size ratio z vary among the blocks of results. Specifically, the presentation is organized into four blocks as follows:

- In section IV A and in Figure 6 structures with $C \geq 1/2$ are shown, for $\rho = 0.6$ and $z = 0.5$.
- In section IV B and in Figure 8, we focus on the case $C < 1/2$, again for $\rho = 0.6$ and $z = 0.5$.
- A comparison with structures of different densities is presented in section IV C and in Figure 9.
- And, finally, structures with smaller diameter ratio $z = 0.3296$ at $\rho = 0.6$ are presented in section IV D and in Figure 10.

In all cases, we have reproduced by our GA the known results for perpendicular fields, refs 8 and 9, offering corroboration to the soundness of our method and independent confirmation of the same, also in view of the fact that our implementation of GA is different than that of refs 8 and 9.

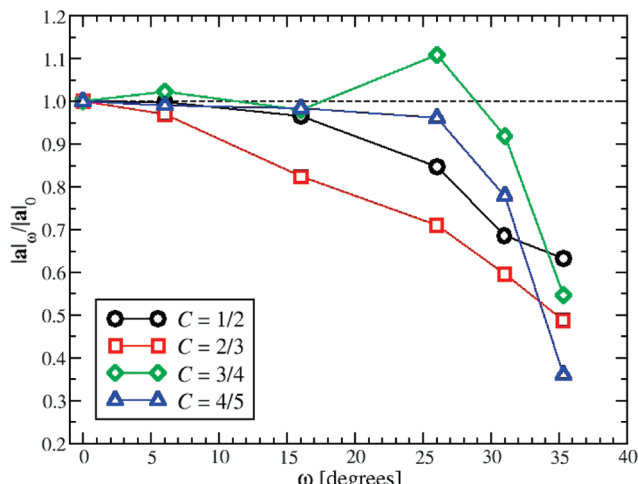


Figure 7. Relative value of the length of the vector $\mathbf{a} = \alpha \mathbf{x}$ for different tilt angles ω , normalized over its value for perpendicular fields, $|\mathbf{a}|_0$. The results pertain to colloidal mixtures of concentrations indicated in the legend and size ratio $z = 0.5$.

A. $C \geq 1/2$. We start with the case $C \geq 1/2$, where the small particles form rather complex structures, as known from the isotropic interaction case.^{8,9} A summary of the results is shown in Figure 6. For the angle range $74^\circ \leq \phi \leq 90^\circ$, we observe mainly that the patterns of the structures are slightly perturbed with respect to the structures obtained for $\phi = 90^\circ$. However, for $\phi < 74^\circ$ the anisotropy becomes significant, and both the small and big particles attempt to take advantage of it by generating new patterns; see Figure 6i,m,n,r,s. At $\phi = 54.7^\circ$ there is no repulsion along the x -axis and the particles form chains parallel to the field, with some unexpected patterns appearing for the composition $C = 3/4$, Figure 6o.

To go into some more detail and obtain a quantitative measure of the anisotropy induced on the structures by the interaction, we consider the length of vector $|\mathbf{a}|$ as a function of the field tilt angle $\omega \equiv 90^\circ - \phi$, so at $\omega = 0$ and $|\mathbf{a}| = |\mathbf{a}|_0$ for perpendicular fields. Naively, one would expect the length of vector \mathbf{a} to monotonically decrease as ω increases but that is not always the case. In Figure 7, we plot precisely the ratio $|\mathbf{a}|_\omega / |\mathbf{a}|_0$ between the length of the primitive lattice vector lying along the x -axis for arbitrary tilt angle ω over the same at $\omega = 0$; according to the conventions put forward in the preceding sections, this describes the relative displacement of the A-type particles of the first lattice along the x -axis, as a function of ω . For all cases, considered, the ratio rapidly decreases as $\omega \rightarrow 35.3^\circ$ ($\phi \rightarrow 54.7^\circ$), since in this limit the dipolar repulsion along the x -axis disappears and the A-particles come into direct contact with one another. The fashion in which this happens depends on the concentration: a flat ratio, rapidly decreasing as $\omega \rightarrow 35.3^\circ$ is approached is observed for $C = 4/5$, whereas smoother, monotonic decreases are seen for $C = 1/2$ and $C = 2/3$. These features underline the role of the small particles in influencing the ordering of the big ones, a characteristic that becomes pronounced for the case $C = 3/4$. Indeed, for this composition, it can be seen that the dependence of the ratio on ω is *nonmonotonic*, and a pronounced maximum is discerned at $\omega = 26^\circ$. As can be seen in Figure 6m that corresponds to this case, this is caused by an unusual ordering between big and small colloids, in which one small colloid *intervenes* between two large ones along the chain formed by the latter, whereas the remaining two small ones order in zigzag types of chains between the aforementioned big/small chains. At the next higher tilt angle, $\omega = 31^\circ$, the zigzag chains have “flattened out” but

the “mixed chain” effect remains; see Figure 6n. Finally, for $\phi \rightarrow 54.7^\circ$, Figure 6o, chains of big and small particles separate but the “memory” of the breakup of the small particles into two subgroups is still there: indeed, there are now *two kinds* of small chains, dense and sparse ones, the former emerging from the pure B-particle chains at smaller tilt angles and the latter from those B-particles that used to intervene between the big ones.

The intervention of a small particle between two big ones along the chain also occurs for concentration $C = 4/5$, Figure 6p-s but it is more intuitive there, since the feature is already present for the isotropic interaction case, Figure 6p. Accordingly, it does not lead to any nonmonotonic behavior of the ratio $|\mathbf{a}|_\omega / |\mathbf{a}|_0$. We also note here that in our initial assumptions of our model, the length of vector \mathbf{a} is always smaller than the length of \mathbf{b} ; this significantly simplifies the problem, it has also the effect to limit the search space. Nevertheless, when the restriction was removed, there was no change in our results. An explanation for this behavior is that the small particles in the unit cell feel first the anisotropy and attempt to come in-between the primary lattice’s particles into a head-tail configuration; compare Figure 6l,m. Additionally, the particles of the primary lattice also attempt to position themselves into a more favorable oblique formation.

Focusing now on the three “normal” cases, $C = 1/2$, $2/3$, and $4/5$, we see that as the angle of the magnetic field is further tilted, the particles of the primary lattice prefer to come closer together, while increasing their separation distance in the y -axis, as seen clearly in the cases $C = 1/2$ and $C = 2/3$, Figure 6d,i. The structures at $\phi = 54.7^\circ$ converge into a series of chains parallel to the magnetic field. As the number of small particles increases, there is no enough space to accompany them all along a single chain, thus new chains are formed; however, the ratio of chain numbers f_B/f_A is *not* the same as that of particles species n_B/n_A ; see, e.g., $f_B/f_A = 2$ but $n_B/n_A = 4$ for the case $C = 4/5$, Figure 6t. The reason lies, evidently, in the fact that B-type particles can approach closer than A-type ones. For the size ratio $z = 0.5$ under consideration here, the distance of closer approach between B-particles is twice as small as that between A-particles, so that the chain ratio is smaller than the particle ratio by a factor 2. Evidently, these findings are sensitive on concentration and size ratio, especially for large tilt angles for which the details of the short-range, steric interaction become important.

B. $C < 1/2$. In the second block of results, $C < 1/2$, the big particles become the majority component and attempt to form hexagonal structures, which are disturbed by the small particles, as seen in Figure 8a,f,k. In particular, at perpendicular field, $\phi = 90^\circ$, the neighbors of small particles form a square, which is also seen as the optimum structure for the system $C = 1/2$; see Figure 6a. Similar to the cases of $C \geq 1/2$, as the field is tilted, the particles will rearrange by taking advantage of the anisotropy.

As anisotropy becomes significant, the particles attempt to form chains, as can be seen in Figure 8c,d,h,i,m,n. The patterns do not change significantly; they are compressed along the x -axis and stretched along the y -axis, since the repulsive interactions along the x -direction weaken. Exception to this is the case $C = 1/3$ at $\phi = 59^\circ$, where the big particles instead of forming two chains they form one. Hence, there are no significant changes in the system’s structure due to the domination of the big particles. The hexagonal structures change to oblique and then to chain-like oblique structures, while the rectangular structures, created by the effects of the small particles, do not show any significant changes.

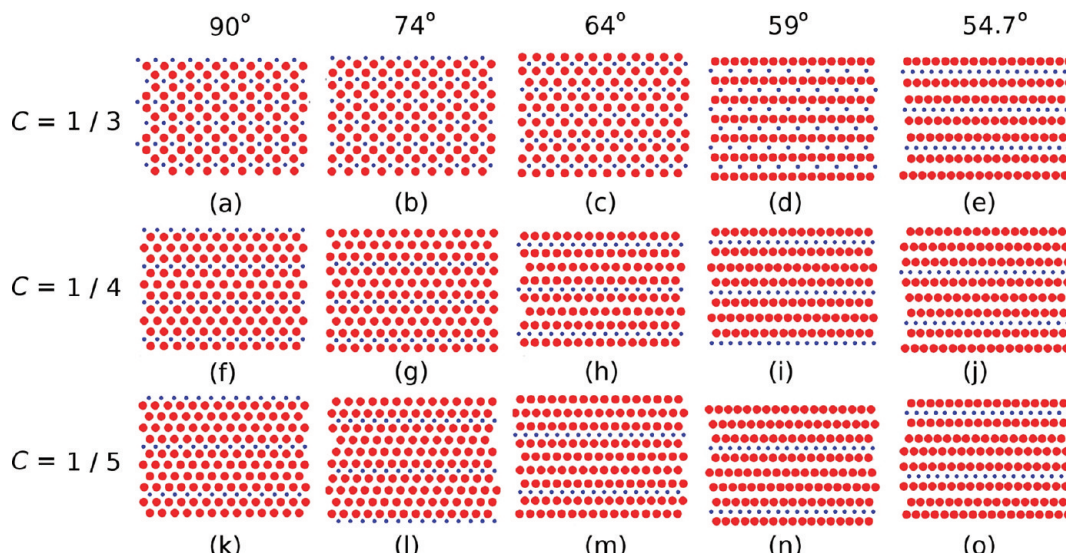


Figure 8. Same as Figure 6 but for concentrations $C < 1/2$.

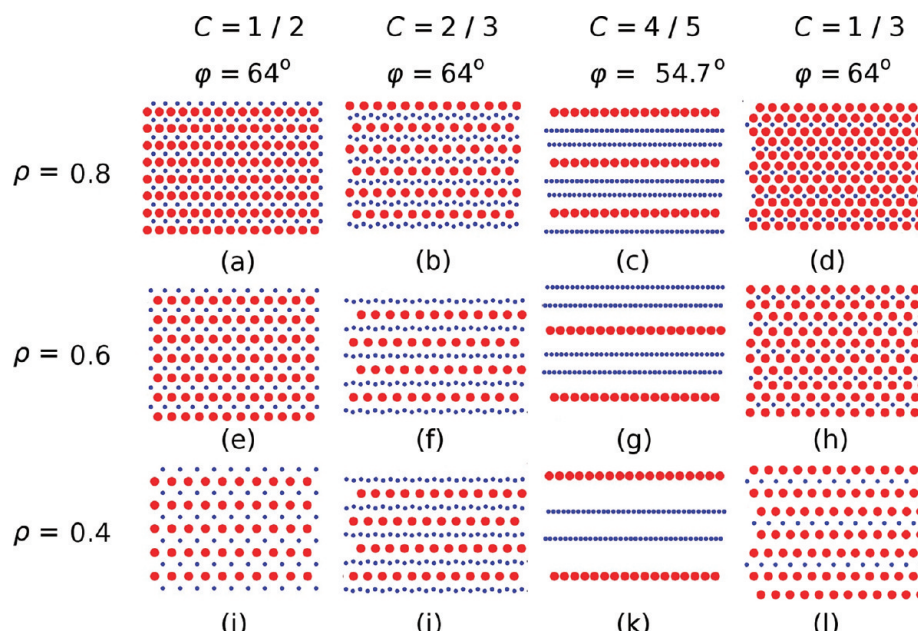


Figure 9. Minimum energy configuration of different compositions as their patterns are affected by density for different values of the composition C and size ratio $z = 0.5$.

At $\phi = 54.7^\circ$ the particles form chains of the same type, aligned parallel to the field. It is interesting to note that parallel chains of particles of A-type form chain-like oblique structures as it has been found for one component systems in ref 28, but if between the chains there is a small particle, then the chains of A-type particles form rectangular structures with the small particle in the middle; cf. Figure 8e,j,o with Figure 6e.

C. Density Effects. In sufficiently dilute concentrations of binary magnetic colloidal mixtures and for sufficiently small tilt angles ω , the distances between the colloids are such that only the dipolar part of the interactions $\Phi_{ij}(\mathbf{r})$ are felt. Accordingly, the pair potentials scale as a power laws at long distances, $\sim r^{-3}$. This feature generates patterns that are *scale-free*, meaning that the overall density is an irrelevant parameter, as shown in previous investigations, where the field was perpendicular to the interface.⁸ Only at higher densities does the excluded volume become a significant factor, and the system ceases to be scale-free. The effects of density should also become visible for strong anisotropies, where the dipolar repulsions along the direction

of \mathbf{B}_{\parallel} are so weak that the steric contribution to the potential becomes important. Therefore, it is pertinent to check the influence of overall concentration on the resulting minimum energy configurations.

In our simulations, we do observe the same patterns for different values of densities for tilted external fields with nonzero interaction along the x -axis. In Figure 9 we present different compositions at different densities with a tilted field, and show how they are affected by anisotropy. In the first example and for composition $C = 1/2$ (see Figure 9a,e,i), the system, for which the magnetic field makes an angle $\phi = 64^\circ$ with the confining plane, remains invariant under change of density. In the second example, we have one more small particle, i.e., for $C = 2/3$, at the same tilt angle, the system changes slightly over different values of density but maintains essentially the same pattern, Figure 9b,f,j. The reason is that at high density, the excluded volume becomes significant and reduces the space between the particles. Therefore, the small particles are unable

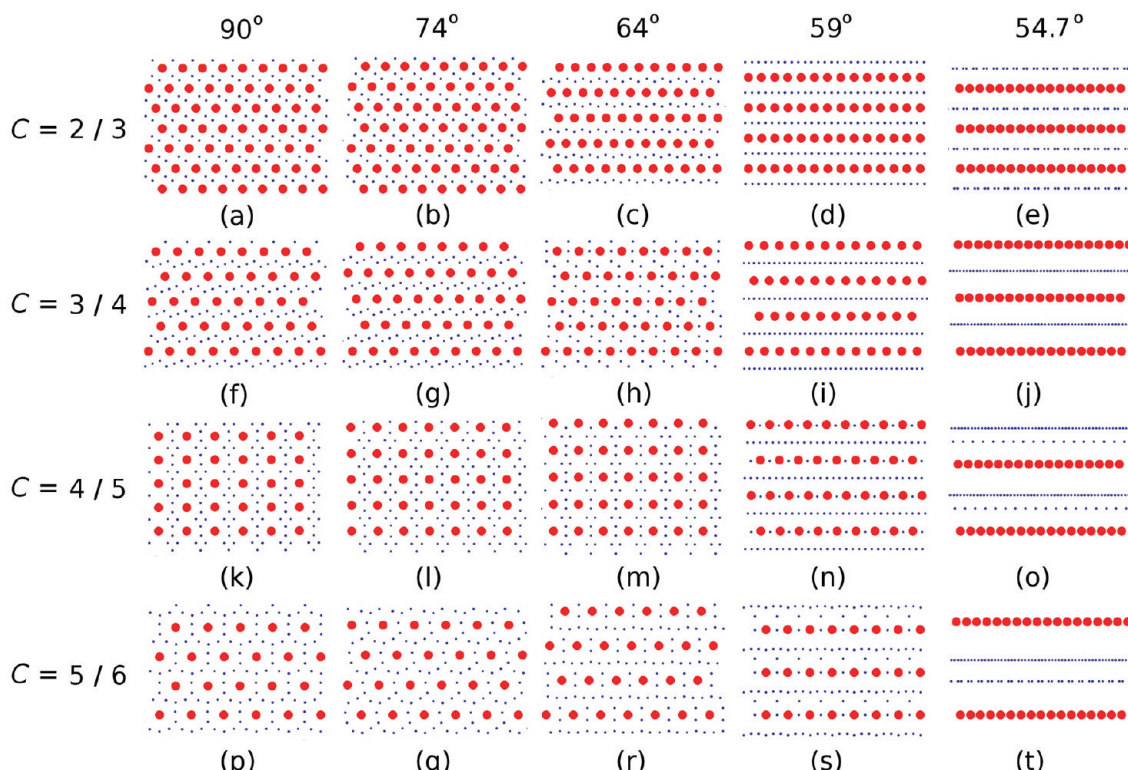


Figure 10. Minimum energy configurations for $C \geq 1/2$, $\rho = 0.6$, and size ratio $z = 0.3296$.

to maintain the pattern they had at lower densities to take advantage of the anisotropy.

In the previous two examples, anisotropy does not affect the system's scale-free features. However, this is true so long there is a repulsive interaction among the particles along the x -axis. At $\phi = 54.7^\circ$ there is no interaction anymore between the particles in the x -direction, which breaks the scale-free property. A characteristic example is shown in Figure 9c,g,k, for the composition $C = 4/5$. As can be seen, the pattern may essentially remain the same, but along the x -axis the particles cease to scale by not changing positions as density changes. A final example is displayed at Figure 9d,h,l, where the composition of the system $C = 1/3$, which has a higher packing fraction than $C = 2/3$; cf. Figure 9b,f,j. The anisotropy, similar to the case $C = 2/3$, does not affect the system being scale-free, until the point there is no interaction in one direction, as it happens for $\phi = 54.7^\circ$.

D. Effects of the Size Ratio. In the final block of results, we look at structures with composition $C > 1/2$, but with smaller diameter ratio than before, $z = 0.3296$. A summary of the results is presented in Figure 10 and should be compared with the same for $z = 0.5$, shown in Figure 6. In general terms and trends, the same behavior with the case $z = 0.5$ is observed as far as the effects of deviations of ϕ from 90° are concerned: initially, the structures are perturbed, then new structures emerge, and at $\phi = 54.7^\circ$ chains are formed. There are, however, some significant quantitative differences that bring forward the importance of the size ratio, and which are discussed below.

The first one occurs for $C = 2/3$ at $\phi = 54.7^\circ$, Figure 10e, where it can be seen that the small particles form a chain, within which they are not equally spaced. In fact, this is a chain of equally spaced pairs but the interpair-spacing is larger than the intrapair one. The phenomenon does not occur for size ratio $z = 0.5$; cf. Figure 6j. The reason behind this difference lies in the fact that the small particles attempt to maximize their distance from the big particles not only along the y -axis but

also along directions lying closer to the x -axis. In the case $z = 0.3296$, the BB-interactions are weaker than for $z = 0.5$ and the steric repulsions also set in at smaller distances, allowing thus the formation of pairs. This effect is not observed for $z = 0.5$, because two small particles cover the distance between two particles of the primary lattice.

Further differences are observed for the concentrations $C = 3/4$ and $C = 4/5$. For the former concentration, the formation of mixed AB-chains as well as of bidisperse B-chains has been observed for $z = 0.5$; see Figure 6m–o. At a smaller size ratio these features disappear from this concentration but they show up at *higher* concentration, $C = 4/5$; see Figure 10n,o. Note that the bidisperse B-chains do not occur for $C = 4/5$ and $z = 0.5$, Figure 6t. Further, exotic configurations, featuring mixed AB-chains, “bridges” of small particles perpendicular to the AB- and the pure B-chains, and bidisperse B-chains show up for the concentration $C = 5/6$; see Figure 10s,t.

The above findings are by no means exhaustive, since the parameter space spanned by concentration, size ratio, and external field angle is vast. However, they bring forward some nontrivial facts about the ordering of binary magnetic colloids in tilted external fields. First, guidance from intuition on the nature of the minimum energy configurations is useless: the system develops strategies to accommodate the competing interactions and the associated frustration that cannot be anticipated. Second, the intuitive feeling that chains will form along the direction of \mathbf{B}_{\parallel} is confined in a generic fashion but the *form*, the *number*, and the *ordering* of these chains is nontrivial. And, third, the complexity of the resulting phases grows tremendously for increasing concentration C of the small particles and for large susceptibility and size asymmetries, a feature already observed, both for the case of isotropic interactions^{8,9} and for the prototype case of binary hard-disk mixtures of different diameters.²¹ In this respect, genetic algorithms are truly indispensable tools in discovering the

nontrivial forms of ordering that emerge in these “simple” colloidal mixtures.

V. Conclusions

We have applied genetic algorithms to study equilibrium configurations of binary mixture of two-dimensional dipolar particles in the presence of a tilted external magnetic field, which introduces anisotropic interactions between the particles. At a small degree of anisotropy, the structures are perturbed, while once the anisotropy reaches the maximum degree, that is, when there is no repulsive (or attractive) interactions along the direction of the magnetic field, the particles form chains aligned parallel to the field. By varying the degree of anisotropy and density, we found a rich spectrum of new structures. Our findings should be experimentally verifiable in setups of mixtures of confined, superparamagnetic colloids⁷ in suitably tilted external fields.⁴³

Acknowledgment. We thank Julia Fornleitner (Vienna and Jülich) for a critical reading of the manuscript and helpful discussions, as well as Gerhard Kahl (Vienna), Peter Keim, and Georg Maret (Konstanz) for helpful discussions. A.C. thanks the Department of Physics of the University of Düsseldorf for its hospitality during a research visit, in which this work has been performed. This work has been supported by the DFG through the Transregional Collaborative Research Center SFB-TR6, “Physics of Colloidal Dispersions in External Fields”, Project Section C3.

References and Notes

- (1) Aveyard, R.; Clint, J. H.; Nees, D.; Quirke, N. *Langmuir* **2000**, *16*, 8820.
- (2) Camp, P. J. *Phys. Rev. E* **2003**, *68*, 061506.
- (3) Zahn, K.; Wille, A.; Maret, G.; Sengupta, S.; Nielaba, P. *Phys. Rev. Lett.* **2003**, *90*, 155506.
- (4) Robinson, D. J.; Earnshaw, J. C. *Phys. Rev. Lett.* **1993**, *71*, 715.
- (5) Hurd, A. J.; Schaefer, D. W. *Phys. Rev. Lett.* **1985**, *54*, 1043.
- (6) Hoffmann, N.; Ebert, F.; Likos, C. N.; Löwen, H.; Maret, G. *Phys. Rev. Lett.* **2006**, *97*, 078301.
- (7) Ebert, F.; Keim, P.; Maret, G. *Eur. Phys. J. E* **2008**, *26*, 161.
- (8) Fornleitner, J.; Lo Verso, F.; Kahl, G.; Likos, C. N. *Soft Matter* **2008**, *4*, 480–484.
- (9) Fornleitner, J.; Lo Verso, F.; Kahl, G.; Likos, C. N. *Langmuir* **2009**, *25*, 7836–7846.
- (10) Bresme, F.; Oettel, M. *J. Phys.: Condens. Matter* **2007**, *19*, 413101.
- (11) Sun, J.; Stirner, T. *Langmuir* **2001**, *17*, 3103.
- (12) Zahn, K.; Lenke, R.; Maret, G. *Phys. Rev. Lett.* **1999**, *82*, 2721.
- (13) Zahn, K.; Maret, G. *Phys. Rev. Lett.* **2000**, *85*, 3656.
- (14) Keim, P.; Maret, G.; Herz, U.; von Grünberg, H. H. *Phys. Rev. Lett.* **2004**, *92*, 215504.
- (15) Eisenmann, C.; Gasser, U.; Keim, P.; Maret, G. *Phys. Rev. Lett.* **2004**, *93*, 105702.
- (16) von Grünberg, H. H.; Keim, P.; Zahn, K.; Maret, G. *Phys. Rev. Lett.* **2004**, *93*, 255703.
- (17) Eisenmann, C.; Gasser, U.; Keim, P.; Maret, G.; von Grünberg, H. H. *Phys. Rev. Lett.* **2005**, *95*, 185502.
- (18) Baumgartl, J.; Zvyagolskaya, M.; Bechinger, C. *Phys. Rev. Lett.* **2008**, *99*, 205503; *Phys. Rev. Lett.* **2008**, *100*, 219903(E).
- (19) Baumgartl, J.; Dietrich, J.; Dobnikar, J.; Bechinger, C.; von Grünberg, H. H. *Soft Matter* **2008**, *4*, 2199.
- (20) Hoffmann, N.; Likos, C. N.; Löwen, H. *J. Phys.: Condens. Matter* **2006**, *18*, 10193.
- (21) Likos, C. N.; Henley, C. L. *Philos. Mag. B* **1993**, *68*, 85–113.
- (22) Adamczyk, Z.; Weronski, P. *J. Colloid Interface Sci.* **1997**, *189*, 348.
- (23) Adamczyk, Z. *J. Colloid Interface Sci.* **2003**, *100*, 267.
- (24) Cahill, B. P.; Papastavrou, G.; Koper, G. J. M.; Borkovec, M. *Langmuir* **2008**, *24*, 465.
- (25) Oberholzer, M. R.; Stankovich, J. M.; Carnie, S. L.; Chan, D. Y. C.; Lenhoff, A. M. *J. Colloid Interface Sci.* **1997**, *194*, 138.
- (26) Oberholzer, M. R.; Wagner, N. J.; Lenhoff, A. M. *J. Chem. Phys.* **1997**, *107*, 9157.
- (27) Herrera-Velarde, S.; von Grünberg, H. H. *Soft Matter* **2009**, *5*, 391.
- (28) Frolov, V. A.; Blaak, R.; Likos, C. N.; Löwen, H. *Phys. Rev. E* **2003**, *68*, 061406.
- (29) Weeks, J. D.; Chandler, D.; Andersen, H. C. *J. Chem. Phys.* **1971**, *54*, 5237.
- (30) Maitland, G. C.; Rigby, M.; Smith, E. B.; Wakeham, W. A. *Intermolecular Forces*; Oxford University Press: Clarendon, 1981.
- (31) Holland, J. H. *Adaption in Natural and Artificial Systems*; MIT Press: Boston, 1992.
- (32) DeJong, K. A. *Foundations of Genetic Algorithms*; Whitley: New York, 1993.
- (33) Michalewicz, Z. *Genetic Algorithms + Data Structures = Evolution Programs*; Springer-Verlag, 1992.
- (34) Gottwald, D.; Kahl, G.; Likos, C. N. *J. Chem. Phys.* **2005**, *122*, 204503.
- (35) Fornleitner, J.; Kahl, G. *Europhys. Lett.* **2008**, *82*, 18001.
- (36) Dobnikar, J.; Fornleitner, J.; Kahl, G. *J. Phys.: Condens. Matter* **2008**, *20*, 494220.
- (37) Pauschenwein, G. J.; Kahl, G. *Soft Matter* **2008**, *4*, 1396.
- (38) Pauschenwein, G. J.; Kahl, G. *J. Chem. Phys.* **2008**, *129*, 174107.
- (39) Goldberg, D. E. *Genetic Algorithms in Search, Optimization, and Machine Learning*; Addison-Wesley: Reading, MA, 1989.
- (40) Cedeno, W.; Vemuri, V. R.; Slezak, T. *Evolutionary Comp.* **1994**, *2*, 321–345.
- (41) Note that the parameters c_1^a and c_1^b are missing, since they have been set to zero. This leaves precisely $2s-2$ parameters from the basis vectors of the lattice, which together with x and Ψ form a chromosome with $2s$ genes.
- (42) Eisenmann, C.; Keim, P.; Gasser, U.; Maret, G. *J. Phys.: Condens. Matter* **2004**, *16*, S4095.
- (43) Note that a zero-temperature system can be realized experimentally by reducing the effective temperature, $\propto k_B T / (\chi B)^2$, via the external magnetic field B (for more details see ref 42). In the case of one-component magnetic colloids, this has been convincingly demonstrated by P. Keim et al.,¹⁴ who crystallized a large enough sample to measure the phonon spectra by means of video microscopy and making use of the equipartition theorem. Finite temperatures are thus not expected to have a dramatic effect, provided $k_B T$ is much lower than the magnetic interaction energy.

JP903820D